Supporting Information

Exploring the Dynamic Behaviour and Optical Properties of Indolocarbazole Charge-Transfer Cocrystals

Jade Cisneros[a], Ernesto A. Hernández-Morales[a], Armando Navarro-Huerta[a], Jan Blahut[b], Erika Bartůňková[b], Simon J. Teat[c], Rubén A. Toscano[a], Martin Dračínský[b]*, Braulio Rodríguez-Molina[a]*

[a] *Instituto de Química, Universidad Nacional Autónoma de México, Circuito Exterior S/N, Ciudad Universitaria, Coyoacán 04510, Mexico City, Mexico.*

[b] *Institute of Organic Chemistry and Biochemistry, Czech Academy of Sciences, 160 00 Prague, Czech Republic.*

[c] *Advanced Light Source, Lawrence Berkeley National Laboratory, Berkeley, California 94720-8229, United States*

*martin.dracinsky@uochb.cas.cz

*brodriguez@iquimica.unam.mx

Contents

Materials and methods

Reagents and solvents were purchased from Sigma-Aldrich and were used without further purification. The 7,7,8,8-tetracyanoquinodimethane was recrystallized with acetone. In all synthesis procedures, column chromatography was used as a purification method, using silica gel (mesh size 230 – 400, average pore size of 60 Å) as the stationary phase and mixtures of hexane/dichloromethane as the mobile phase. Reactions were monitored through TLC using silica gel plates 60 GF_{254} purchased from Merck and spots were detected by UV-light absorption. Solution ^{1}H and ^{13}C experiments were recorded at room temperature using Bruker Avance III 400. The spectroscopic data is referenced to $CDCl_3$. High-Resolution Mass Spectrometry was obtained in a Jeol JMS-AccuTOF JMS-T100LC spectrometer, ionization mode: Direct Analysis in Real Time (DART). FTIR spectra experiments were recorded with Bruker Tensor-27 ATR equipped with a diamond tip in the spectral window from 4000 to 400 cm^{-1}. Melting points were determined in a Fisher-Jones melting point apparatus. Powder X-ray diffraction analyses were carried out using a Bruker D8 Advance diffractometer with CuKα radiation at 1.5418 Å and a LinxEye detector. Operating at 30 kV and 25 mA, the 2θ scanning range was from 5 to 50° with a step size of 0.03° and a time per step of 0.3 s. The DSC/TGA were recorded in a Netzsch model STA 449 F3 Jupiter, under a nitrogen atmosphere and heating rate of 10 °C/min from 25 °C to 400 °C. The UV-Vis absorption analyses were obtained using a Perkin-Elmer spectrometer Lamba 900 with the diffuse reflectance technique. Single crystal X-ray diffraction analyses were obtained using a Bruker APEX-II or D8Venture CCD diffractometer with CuKα or MoKα radiation. The data was refined using SHEXL-2019/3 software. The B-level alerts found in the checkCIF report for ICZ structure are due to the poor diffraction quality of the crystal, mainly caused by its size and morphology. Solid-state NMR experiments were performed on a JEOL 600 MHz spectrometer at a 14.1 T field corresponding to a 600 MHz ^{1}H Larmor frequency, equipped with a 3.2 mm HX probe. The sample was packed in a 3.2 mm zirconia rotor. The $^{13}C\{^{1}H\}$ spectra were acquired using cross-polarization experiment with 5 ms mixing time and pre-acquisition delay set to $1.5\times T_1$ (^{1}H) (as ^{1}H obtained from saturation recovery experiment). The T_1 (^{19}F) was determined under static conditions using saturation recovery experiment with spin-echo detection. At high temperature $T_{set} \geq 25$ ˚C the signal of **TFBQ** was resolved from signal of probe background, and saturation-recovery data were therefore fitted using three-parameter exponential function. At lower temperature the signal of **TFBQ** overlaps with the background and, therefore, the data were fitted using double-exponential function with one of the relaxation times fixed on 2.2 s i.e. T_1 (^{19}F) of probe background determined separately. Real sample temperature were determined using chemical shift of ^{207}Pb (at 18 kHz MAS and 1 kHz for static case).[S1] All raw data are available in Zenodo archive. [https://doi.org/10.5281/zenodo.15017371]. The periodic DFT geometry optimizations were performed using the CASTEP program,[S2] version 22.11, which uses pseudopotentials to model the effects of core electrons and plane waves to describe valence electrons. The unit-cell parameters were fixed, the electronic potential energy surface was modeled using the functional PBE.[S3] The optimizations were performed utilizing the plane-wave basis-set energy cutoff of 600 eV, default ultrasoft[S4] “on-the-fly” generation of

pseudopotentials, a minimum *k*-point spacing of 0.1 $Å^{-1}$ over the Brillouin zone via a Monkhorst–Pack grid,[S5] and empirical dispersion corrections using the TS correction scheme.[S6] Molecular clusters were extracted from the optimized crystal structures. The clusters consisted of the central **TFBQ** molecule and all surrounding molecules with contacts shorter than the sum of vdW radii. Rotamers of the cocrystals with the central molecule rotated by +60 and −60° were created and the geometries of the central molecule in these clusters were optimized at the DFT level using Gaussian16 software,[S7] the B3LYP functional[S8,S9] and 3-21g basis set. The positions of all atoms in the cluster except the central **TFBQ** molecule were fixed. The transition-state structures were searched using the QST3 method.

Synthesis of compounds

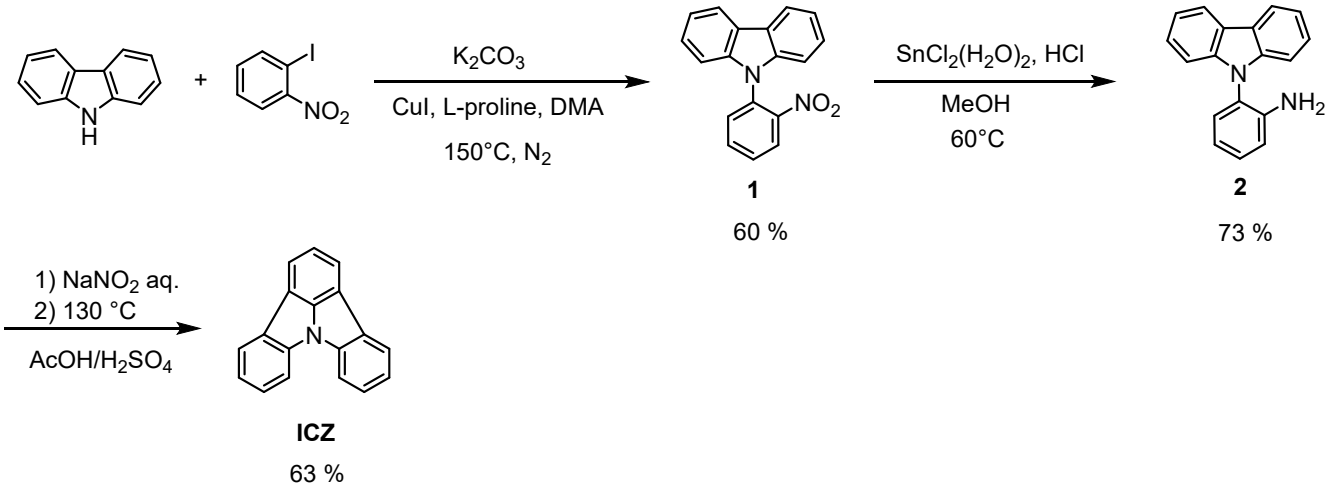

Scheme S1. General procedure of the synthesis of **ICZ.**

9-(2-nitrophenyl)-9H-carbazole (1)

In a two-neck round-bottom flask with magnetic stirrer 9H-carbazole (300 mg, 1.79 mmol, 1 eq), 1-iodo-2-nitrobenzene (670 mg, 2.69 mmol, 1.5 eq), potassium carbonate (1.12 g, 8.07 mmol, 4.5 eq), copper(I) iodide (25.6 mg, 0.13 mmol, 5% mol), L-proline (5.2 mg, 0.04 mmol, 1.7% mol) were added in dry *N,N*-dimethylacetamide (10 mL) and degassed with N_2. The mixture was heated at 150 °C for 40 hours. After cooling down to room temperature, the mixture was diluted with ethyl acetate and washed with water (3x10 mL). The solvent was removed by rotatory evaporation and the compound **1** was purified by silica gel column chromatography with 3 mL of triethylamine, followed by a mixture of hexane/dichloromethane (95:5). The product was recovered as a yellow solid. (0.307 g, **yield 60%**, **m.p.** 150-155 °C). **^{1}H NMR** (500 MHz, $CDCl_3$) δ: 8.17 (dd, *J* = 8.5, 1.5 Hz, 1H), 8.13 (dt, *J* = 7.8, 0.9 Hz, 2H), 7.84 (td, *J* = 7.8, 1.5 Hz, 1H), 7.68 (ddd, *J* = 8.2, 6.5, 1.5 Hz, 2H), 7.39 (ddd,

J = 8.3, 7.1, 1.3 Hz, 2H), 7.30 (td, *J* = 7.5, 1.0 Hz, 2H), 7.11 (dt, *J* = 8.2, 0.9 Hz, 2H). **^{13}C NMR** (126 MHz, $CDCl_3$) δ: 147.44, 140.79, 134.24, 131.44, 131.32, 129.15, 126.34, 125.97, 123.87, 120.69, 120.59, 109.07. **FTIR** (ATR, cm^{-1}) ν_{max}: 3048, 1945, 1909, 1876, 1824, 1790, 1602, 1524, 1451, 1349, 1227, 848, 781, 749, 633, 433. **HRMS** (DART): *m/z* $[C_{18}H_{13}N_2O_2]+$, calculated 289.09770, found 289.09743, |Δ (*m/z*)| (ppm): 0.96.

2-(9H-carbazole-9-yl)aniline (2)

In a round-bottom flask 9-(2-nitrophenyl)-*9H*-carbazole (300 g, 1.04 mmol, 1 eq.) was dissolved in methanol (10 mL). $SnCl_2{\cdot}(H_2O)_2$ (1.17 g, 5.20 mmol, 5 eq.) was used as reducing agent in 5 mL if concentrated 33% HCl. The mixture was heated at 70 °C for 5 hours. After cooling down to room temperature, the reaction mixture was extracted with ethyl acetate and the solution was left to crystallize at 0 °C. The compound **2** was filtered and washed with cold hexane. The product was recovered as a white solid. (0.196 g, **yield 73%**, **m.p.** 110-115 °C). **^{1}H NMR** (400 MHz, $CDCl_3$) δ: 8.15 (dt, *J* = 7.7, 1.0 Hz, 2H), 7.40 (ddd, *J* = 8.3, 7.1, 1.2 Hz, 2H), 7.35 – 7.21 (m, 4H), 7.18 (dt, *J* = 8.2, 0.9 Hz, 2H), 6.98 – 6.84 (m, 2H), 3.30 (s, 2H). **^{13}C NMR** (101 MHz, $CDCl_3$) δ: 144.13, 140.75, 129.75, 129.72, 126.12, 123.46, 122.43, 120.44, 119.98, 118.99, 116.67, 110.25. **FTIR** (ATR, cm^{-1}) ν_{max}: 3472, 3381, 3051, 1609, 1500, 1446, 1311, 1228, 1176, 745, 724, 626, 526, 423. **HRMS** (DART): *m/z* $[C_{18}H_{15}N_2]+$, calculated 259.12352, found 259.12413, |Δ (*m/z*)| (ppm): 2.34.

Indolo[3,2,1-jk]carbazole (ICZ)

To a solution of 2-(*9H*-carbazole-9-yl)-aniline (50 mg, 0.19 mmol, 1 eq.) in AcOH:H_2SO_4 10:1 %v/v (1.5 mL) mixture was added dropwise an aqueous solution of sodium nitrite (20 mg, 0.29 mmol, 1.5 eq in 2.5 mL water) over a period of 20 min. The temperature of the mixture was maintained below 10 °C while addition. The mixture was stirred at 10°C for 15 min and then stirred at 130 °C for 24 h. The reaction mixture was cooled to room temperature and was diluted with ethyl acetate and washed with water (3x10 mL). The solvent was removed by rotatory evaporation and the compound **ICZ** was purified by silica gel column chromatography eluted with hexane. The product was recovered as a white solid. (0.027 g, **yield 63%, m.p.** 136-140 °C) **^{1}H NMR** (500 MHz, $CDCl_3$) δ: 8.15 (dt, *J* = 7.8, 1.0 Hz, 2H), 8.05 (d, *J* = 7.4 Hz, 2H), 7.92 (dt, *J* = 8.1, 0.9 Hz, 2H), 7.62 – 7.52 (m, 3H), 7.36 (td, *J* = 7.6, 1.0 Hz, 2H). **^{13}C NMR** (126 MHz, $CDCl_3$) δ: 143.80, 138.76, 130.08, 126.74, 123.19, 122.86, 121.72, 119.43, 118.50, 112.19. **FTIR** (ATR, cm^{-1}) ν_{max}: 3045, 2922, 2852, 1922, 1893, 1840, 1775, 1601, 1431, 1339, 1121, 793, 748, 683, 422. **HRMS** (DART): *m/z* $[C_{18}H_{12}N]+$, calculated 242.09697, found 242.09697, |Δ (*m/z*)| (ppm): 0.00.

Preparation of cocrystals

Cocrystal ICZ-TCNQ

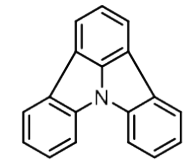

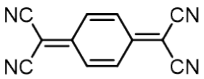

In a 4 mL vial 5 mg of ICZ (20.72 μmol, 1 eq), 4.23 mg of TCNQ (20.72 μmol, 1 eq) were added, then heated up to 90 °C until dissolved in acetone, then stop the heating and left cool to room temperature, after 3-5 days acicular black crystals were obtained.

Cocrystal ICZ-TFBQ

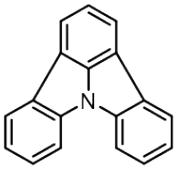

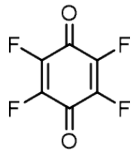

In a 4 mL vial 5 mg of ICZ (20.72 μmol, 1 eq), 3.73 mg of TFBQ (20.72 μmol, 1 eq) were added, then heated up to 90 °C until dissolved in acetone, then stop the heating and left cool to room temperature, after 3-5 days prismatic black crystals were obtained.

Table S1. Crystal structure parameters for **ICZ** at 300 K.

Identification code	**ICZ**	
Empirical formula	$C_{18}H_{11}N$	
Formula weight	241.28	
Temperature (K)	298(2)	
Wavelength (Å)	1.54178	
Crystal system	Orthorhombic	
Space group	*Pca*2$_1$	
Unit cell dimensions	a = 26.734(2) Å	$\alpha = 90°$
	b = 5.1426(4) Å	$\beta = 90°$
	c = 35.293(3) Å	$\gamma = 90°$
Volume (Å^3)	4852.1(6)	
Z	16	
Density (mg m^{-3})	1.321	
Absorption coefficient (mm^{-1})	0.593	
F(000)	2016	
Crystal size (mm^3)	0.417 x 0.064 x 0.046	
Theta range for data collection	2.504 to 70.048°	
Index ranges	-22 ≤ h ≤ 32 -6 ≤ k ≤ 6	

	$-30 \leq l \leq 42$
Reflections collected	36911
Independent reflections	7184 [R(int) = 0.0847]
Completeness to theta = 25.242°	99.6 %
Absorption correction	Semi-empirical from equivalents
Max. and min. transmission	0.7535 and 0.6176
Refinement method	Full-matrix least-squares on F^2
Data / restraints / parameters	7184 / 1 / 685
Goodness-of-fit on F^2	1.276
Final R indices [I>2sigma(I)]	R1 = 0.1539 wR2 = 0.3345
R indices (all data)	R1 = 0.1985 wR2 = 0.3855
Absolute structure parameter	1.6(10)
Extinction coefficient	n/a
Largest diff. peak and hole ($e.Å^{-3}$)	0.990 and -0.485

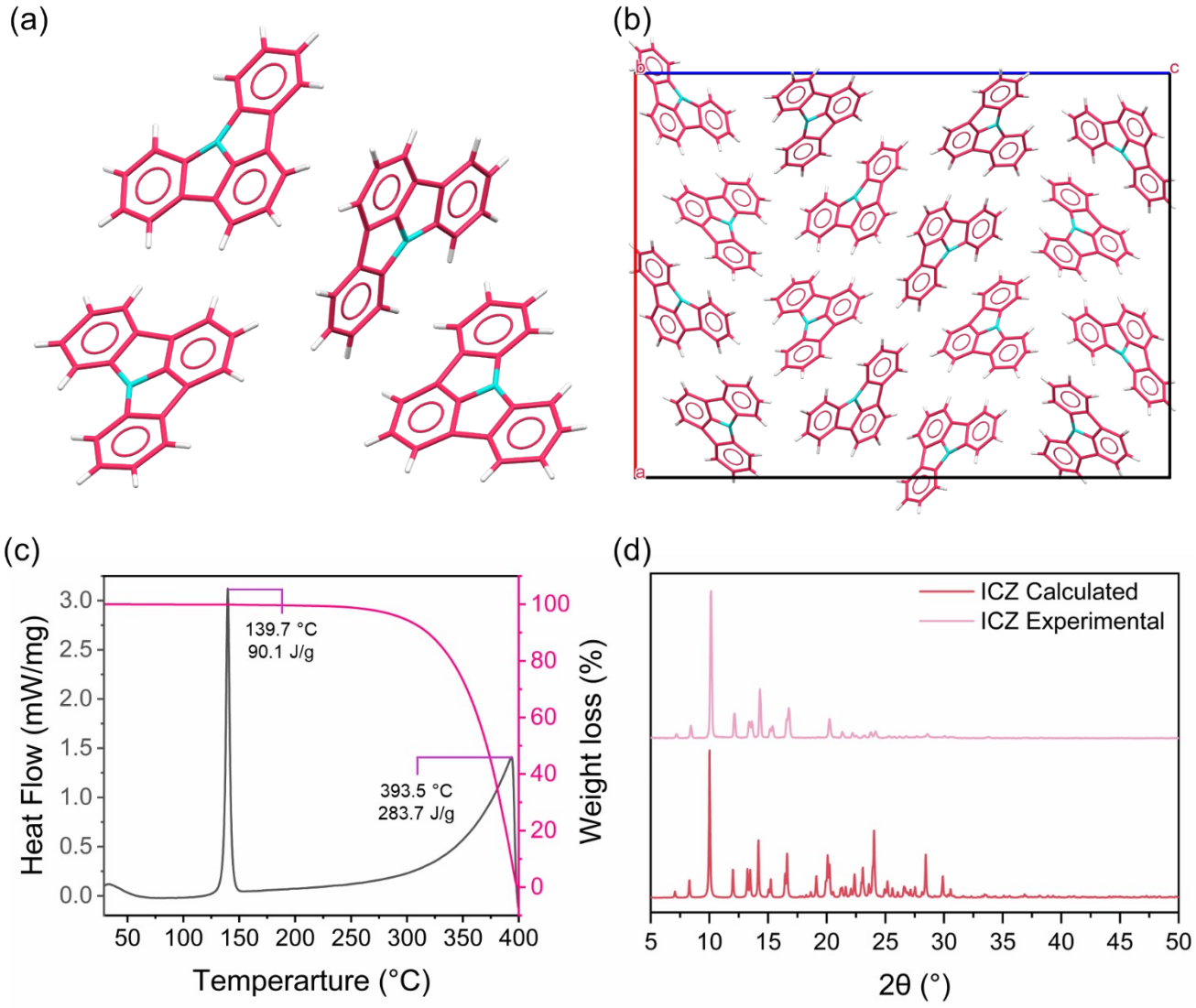

Figure S1. (a) Single-crystal structure of **ICZ**. (b) Unit cell of **ICZ** along *b*-axis. (c) Coupled DSC and TGA of **ICZ** powder. (d) PXRD diffractogram of **ICZ** calculated and experimental.

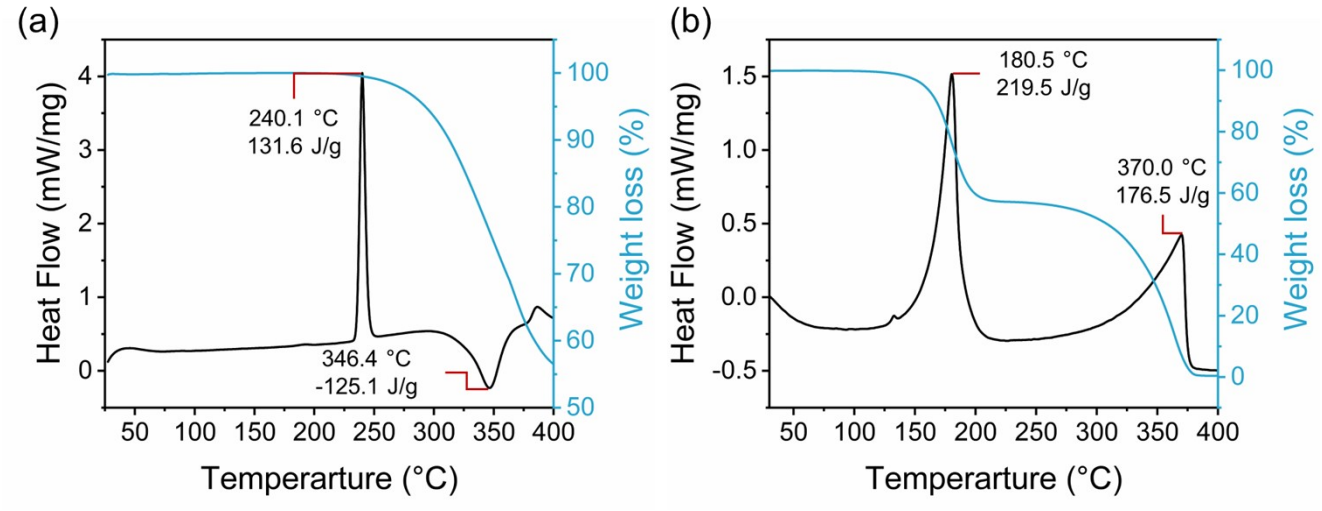

Figure S2. Coupled DSC and TGA analysis of each cocrystal: (a) **ICZ-TCNQ** and (b) **ICZ-TFBQ**.

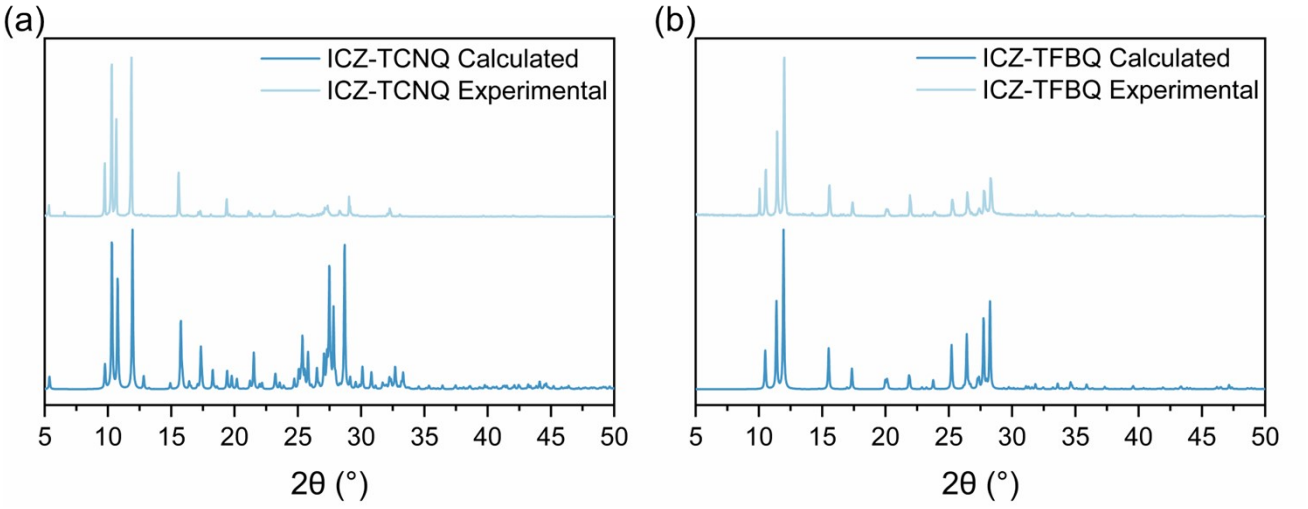

Figure S3. PXRD patterns of each cocrystal calculated and experimental for (a) **ICZ-TCNQ** and (b) **ICZ-TFBQ** cocrystal.

Degree of Charge Transfer

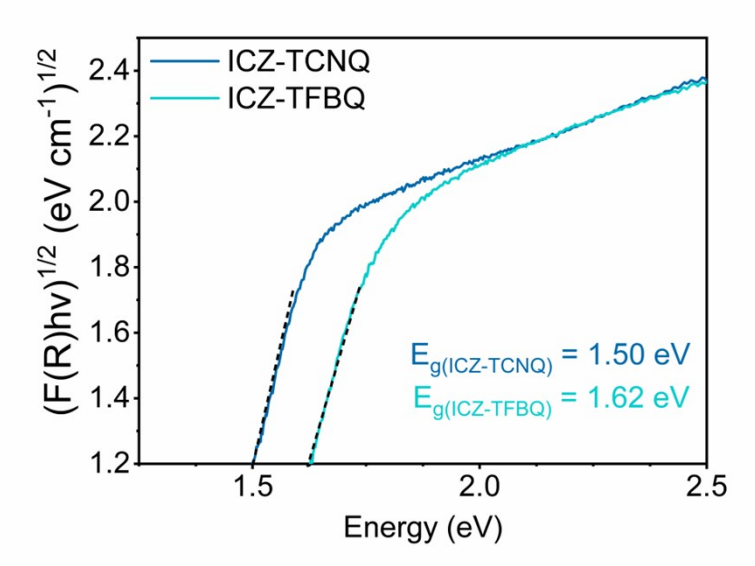

Figure S4. Modified Tauc plot obtained from diffuse reflectance UV-vis spectroscopy.

The calculations of the degree of charge transfer (DCT) were carried out using equation 1. This model assumes that, in an ideal charge transfer process, a 100 % electron transfer from the donor to the acceptor would be achieved. However, this depends on the ionization energy of the donor and the electron affinity of the acceptor. Therefore, the vibrational modes of the acceptor radical anion, which represents an ideal CT process and the vibrational modes of the neutral acceptor, which indicates no CT process are considered. The vibrational frequencies of the CT complex are analyzed, where the DCT for the CT complex must exceed a value of 0.03.[S10]

DCT values for each cocrystal were calculated from Equation 1:

$$DCT = \frac{2\,\Delta v}{v_0}\left(1 - (v_1^2/v_0^2)\right)^{-1} \qquad (1)$$

where $\Delta v = v_0 - v_{CT}$ with v_0, v_{CT} and v_1 representing the stretching frequencies of the neutral acceptor, the CT complex and the acceptor's anion, respectively.

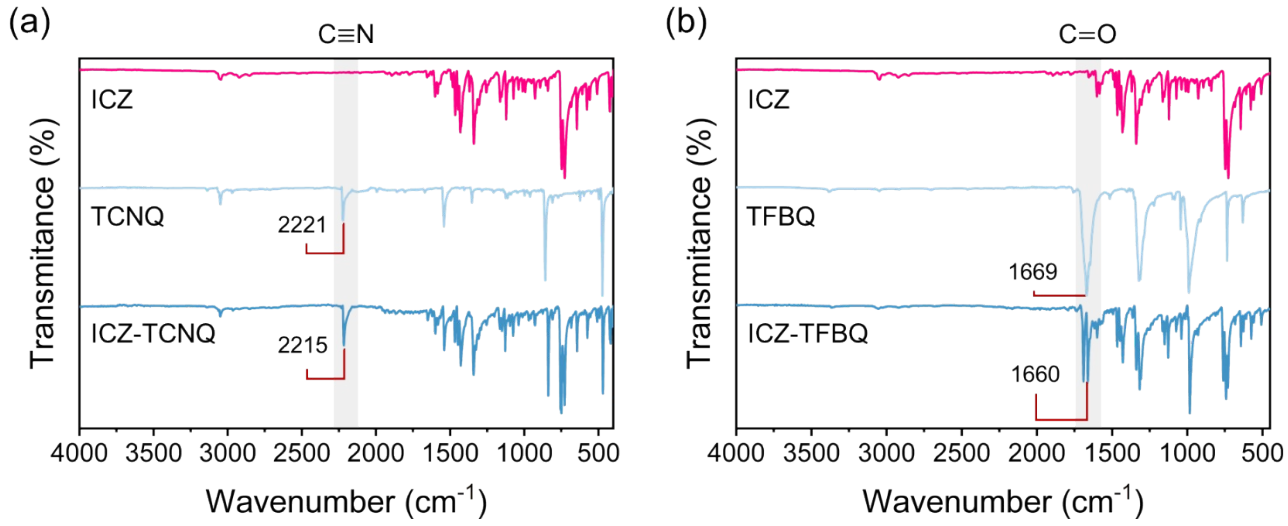

Figure S5. (a) FTIR spectra of **ICZ**, **TCNQ** and **ICZ-TCNQ**. (b) FTIR spectra of **ICZ**, **TFBQ** and **ICZ-TFBQ**. It focuses on the vibrational mode of the cyano or carbonyl group in the coformer and the cocrystal, respectively.

Table S2. Stretching mode values used in the DCT calculation for each cocrystal.

Cocrystal		$v_0\ (cm^{-1})$	$v_{CT}\ (cm^{-1})$	$v_1\ (cm^{-1})$	**DCT**
ICZ-TCNQ	C ≡ N	2221	2215	2199 [S11]	0.27
ICZ-TFBQ	C = O	1669	1660	1520 [S12]	0.06

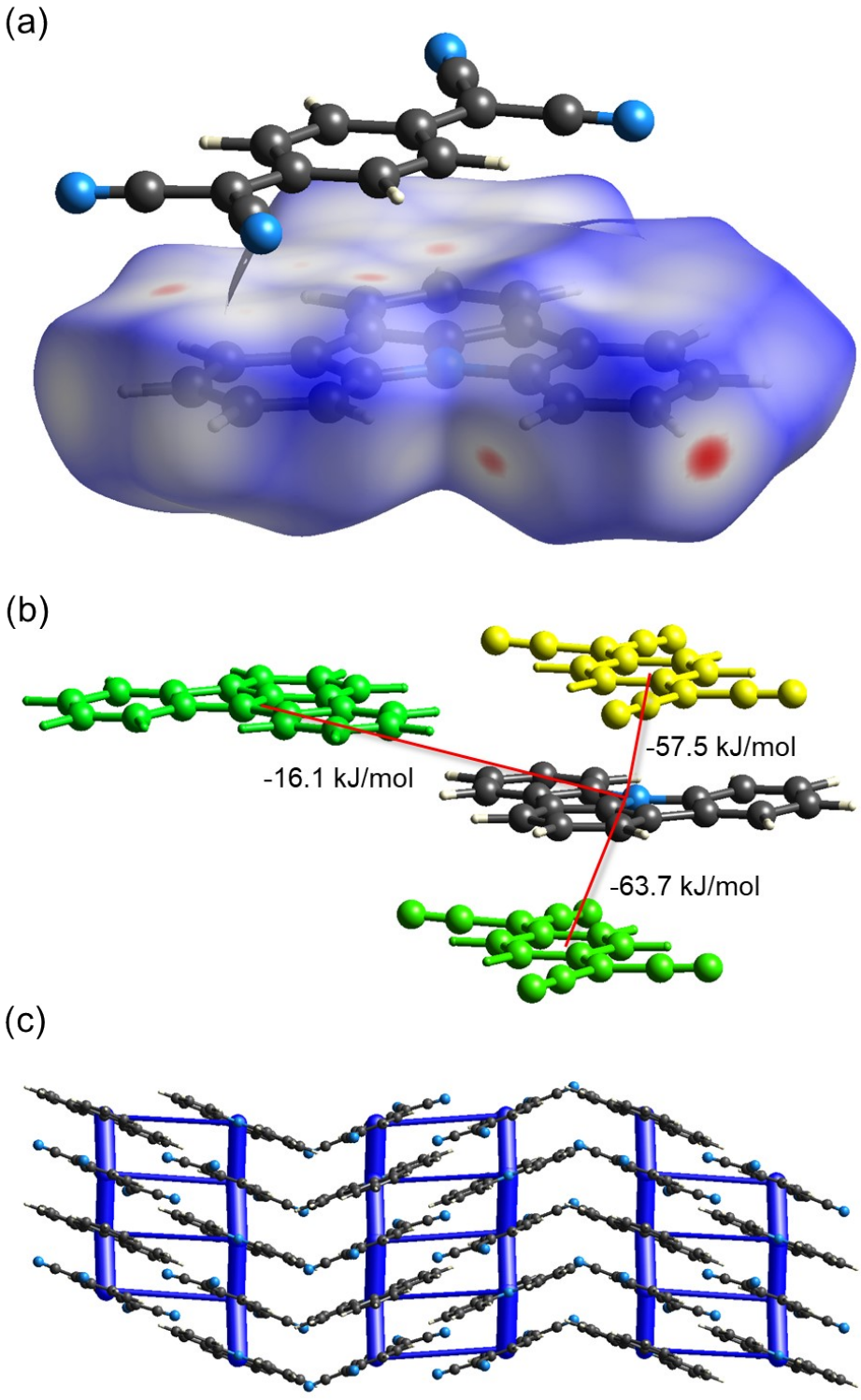

Figure S6. (a) Hirshfeld surface of **ICZ** plotted with d_{norm}. (b) Calculated total interaction energies between one **ICZ** molecule and its surrounding acceptor molecules. (c) Energy frameworks all over **ICZ-TCNQ** packing.

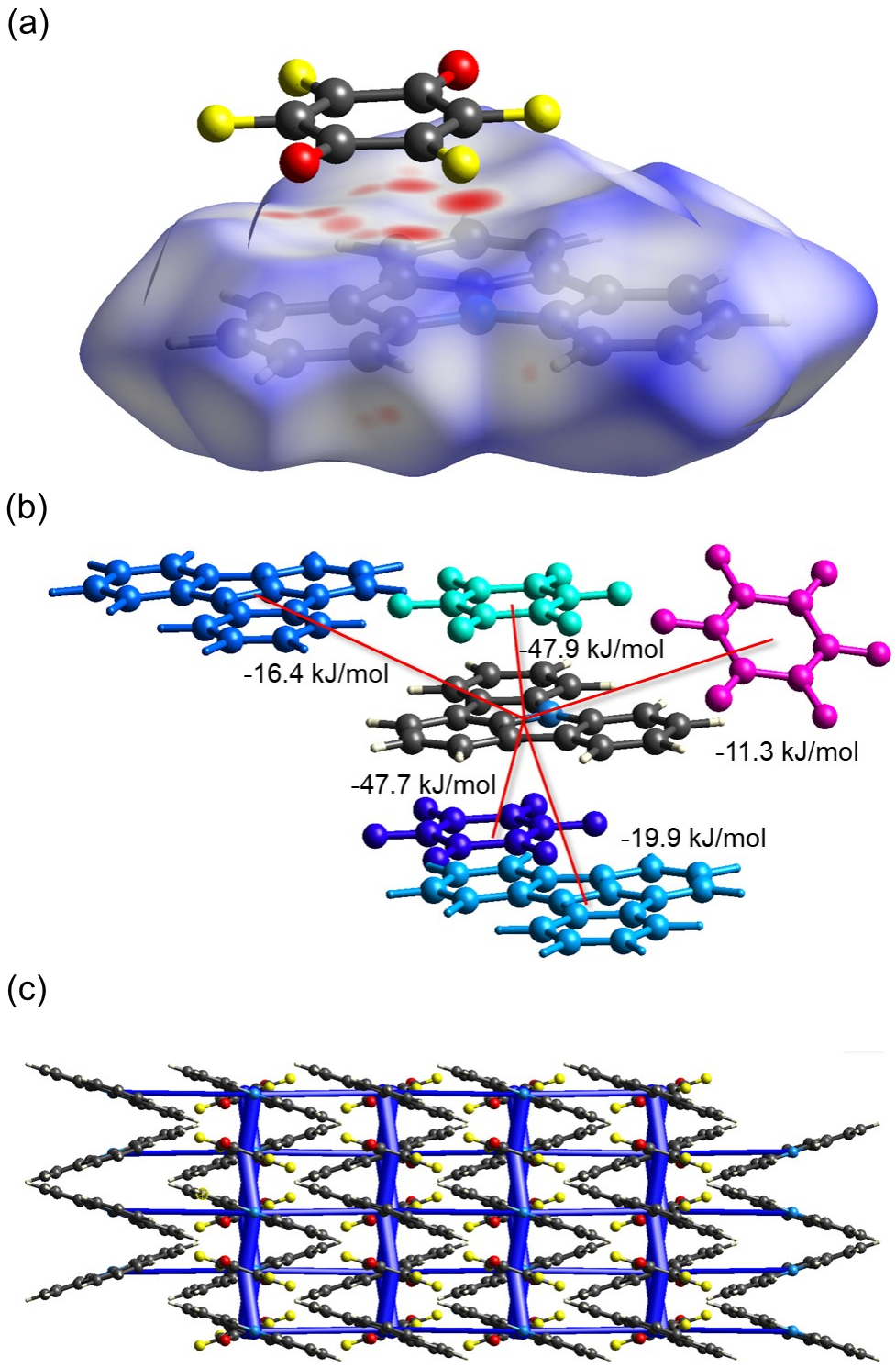

Figure S7. a) Hirshfeld surface of **ICZ** plotted with d_{norm}. (b) Calculated total interaction energies between one **ICZ** molecule and its surrounding acceptor molecules. (c) Energy frameworks all over **ICZ-TFBQ** packing.

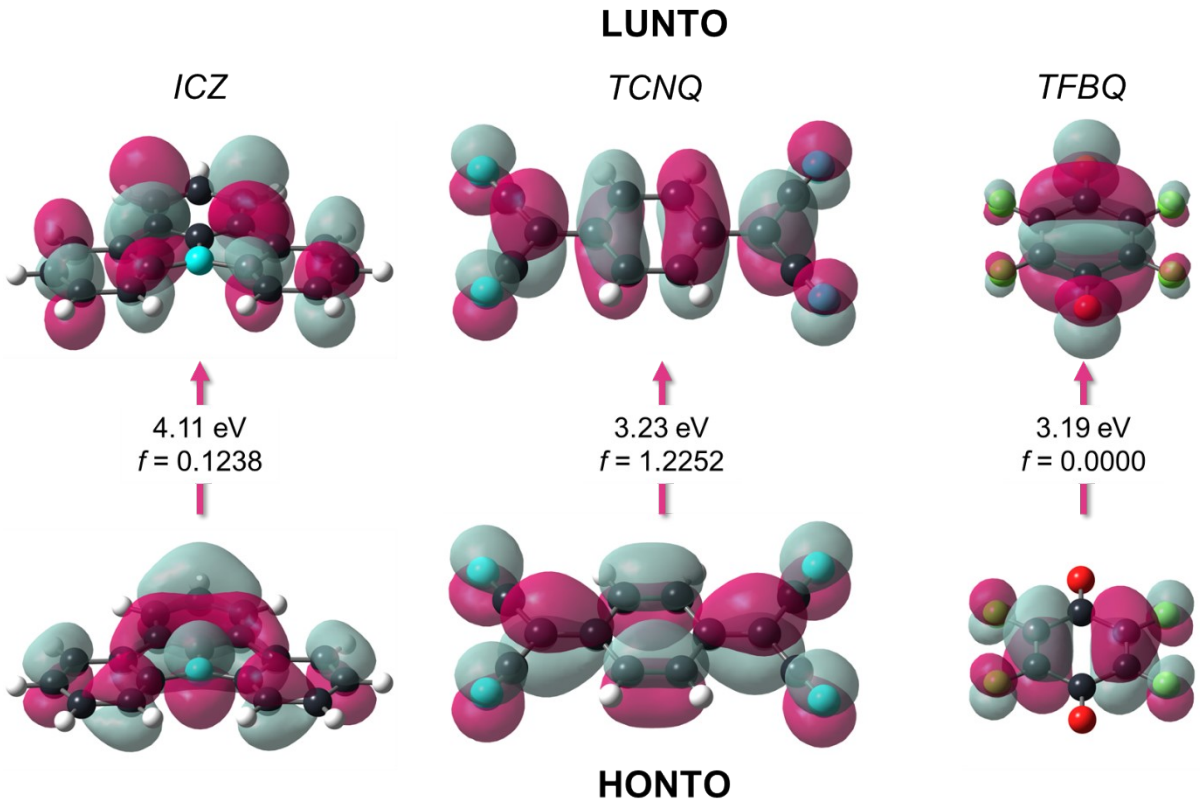

Figure S8. Natural transition orbitals (NTOs) of starting materials **ICZ, TCNQ** and **TFBQ** using TDDFT with CAM-B3LYP functional at the 6-311+G(d,p) level of theory. The associated energies (in eV) and oscillator strengths (*f*) are included.

Photothermal conversion measurements

Photothermal conversion measurements and calculations were conducted following the methodology described by Navarro-Huerta and others.[S13] For each cocrystal, a polycrystalline powdered sample was placed in a quartz sheet (25.4 mg of **ICZ-TCNQ** and 67.6 mg of **ICZ-TFBQ**). The samples were irradiated with an 808 nm red dot laser equipped with a focusing lens (Class IIIb). Temperature measurements were recorded at 1-second intervals using a Flir One GEN3 thermal imaging camera connected to a Samsung C-port. The specific heat capacity (Cp) of each cocrystal was determined using a TA Instruments Thermogravimetric Analyzer employing the Sapphire method. Based on **Figure S10**, the mean Cp value was calculated for each cocrystal before any phase transition. Therefore, the Cp values for the different cocrystals and the quartz sheets are 1.45 J g^{-1} $°C^{-1}$ for **ICZ-TCNQ** and 1.02 J g^{-1} $°C^{-1}$ for **ICZ-TFBQ**. Photothermal conversion efficiency (PTCE) can be calculated as equation 2:

$$\eta = \frac{hS\Delta T_{max}}{I\left(1 - 10^{-A_\lambda}\right)} \qquad (2)$$

Tabla S3. Summary of the values for Photothermal Conversion experiments for each cocrystal.

ICZ-TCNQ (Power density $I = 0.5\ W/cm^2$)			
Cycle	$\tau_s\ (s)$	$\Delta T_{max}\ (°C)$	η
1	66.70	16.8	11.5
2	62.32	16.7	12.3
3	74.81	17.1	10.5
4	57.50	17.2	13.7
5	49.18	17.3	16.1
$\bar{\eta}$ (%)	12.8 ± 2.1		

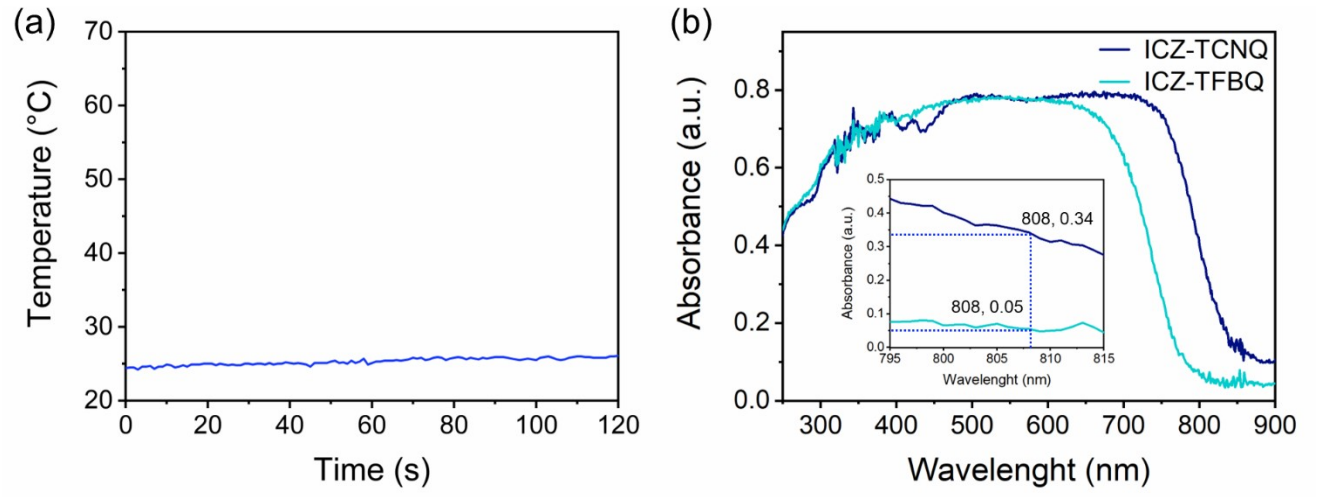

Figure S9. (a) Temperature change of blank under 0.5 W/cm² irradiation. (b) Absorption spectra of cocrystals with absorption values at 808 nm.

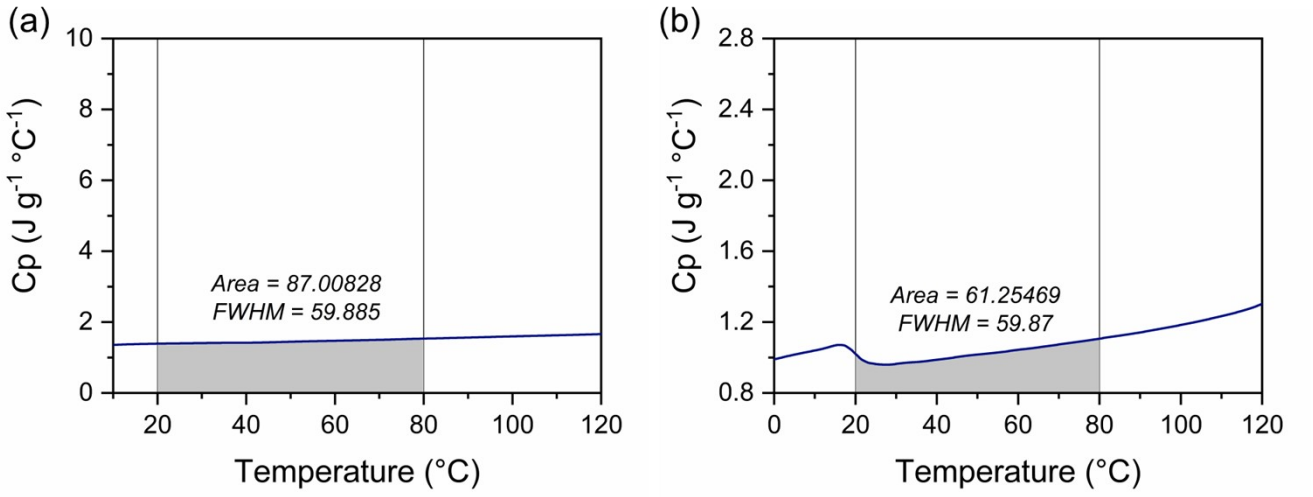

Figure S10. Specific heat capacity (Cp) measurements for (a) **ICZ-TCNQ** and (b) **ICZ-TFBQ** cocrystals.

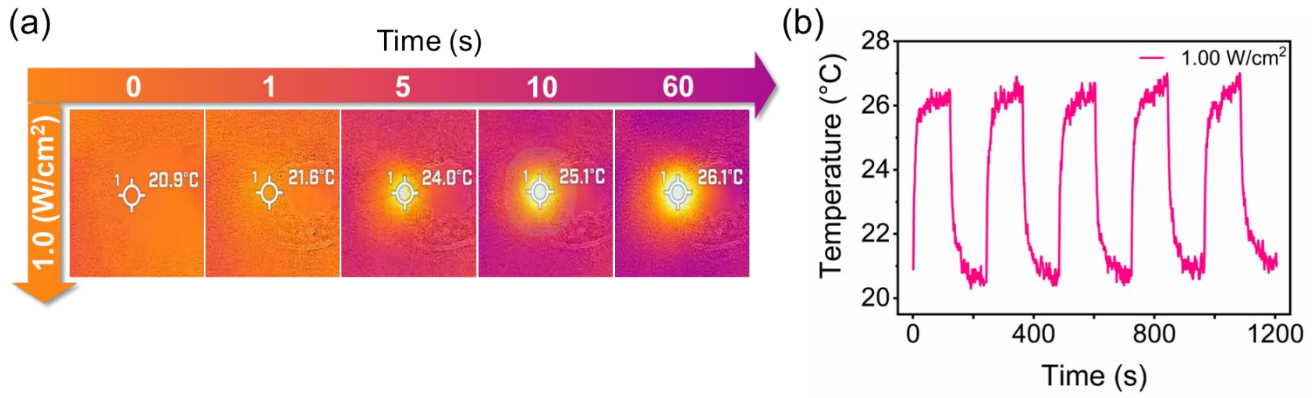

Figure S11. (a) **ICZ-TFBQ** under heating at 1.0 W/cm^2 density power. (b) Heating-cooling curves for **ICZ-TFBQ**.

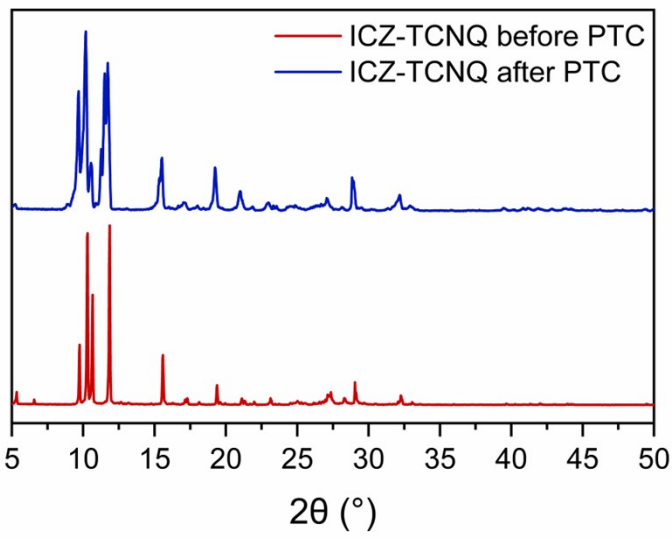

Figure S12. PXRD patterns of **ICZ-TCNQ** cocrystal before and after photothermal conversion experiments.

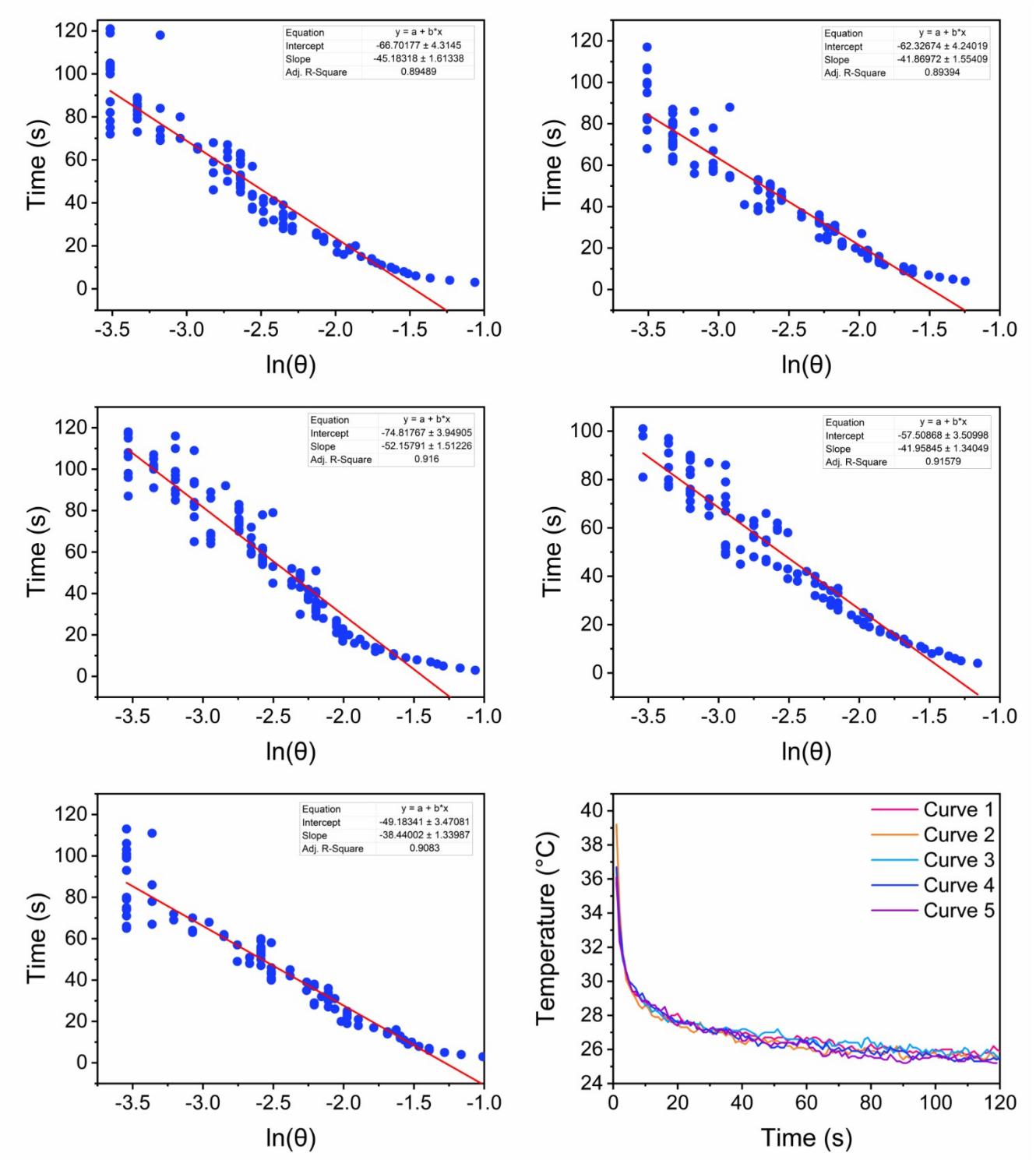

Figure S13. Linear fitting of time as function of the heat transfer coefficient and cooling curves of **ICZ-TCNQ** at 0.5 W/cm^2.

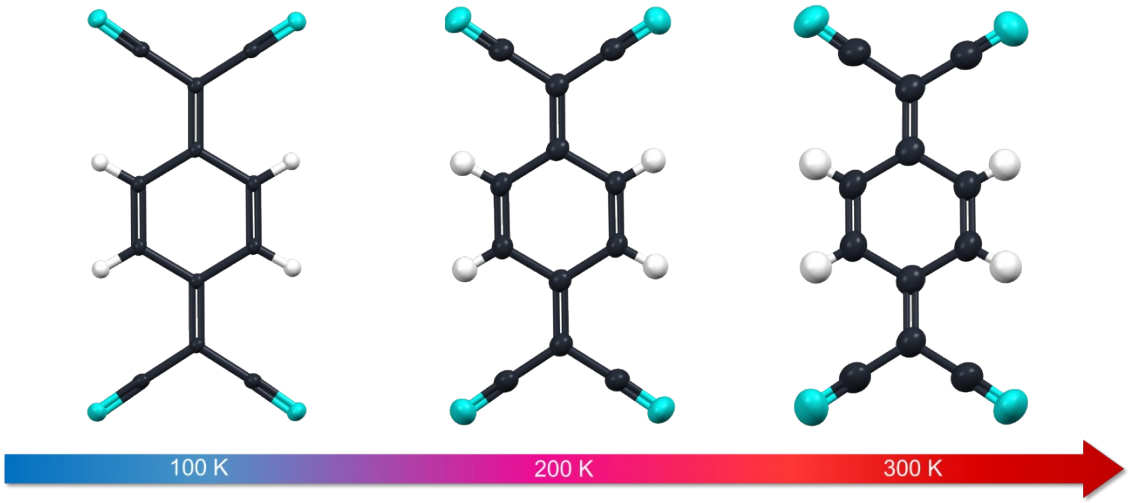

Figure S14. VT-SCXRD of **ICZ-TCNQ** cocrystal at 100 K, 200 K and 300 K.

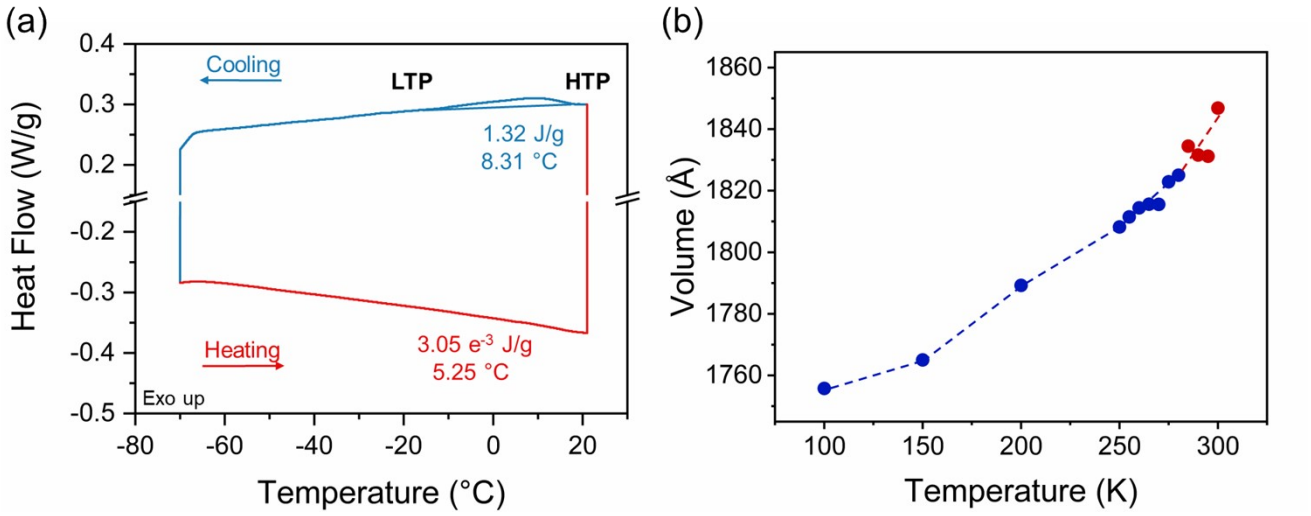

Figure S15. (a) DSC from **ICZ-TFBQ** cocrystal at low temperatures. (b) Cell volume changes as function of temperature.

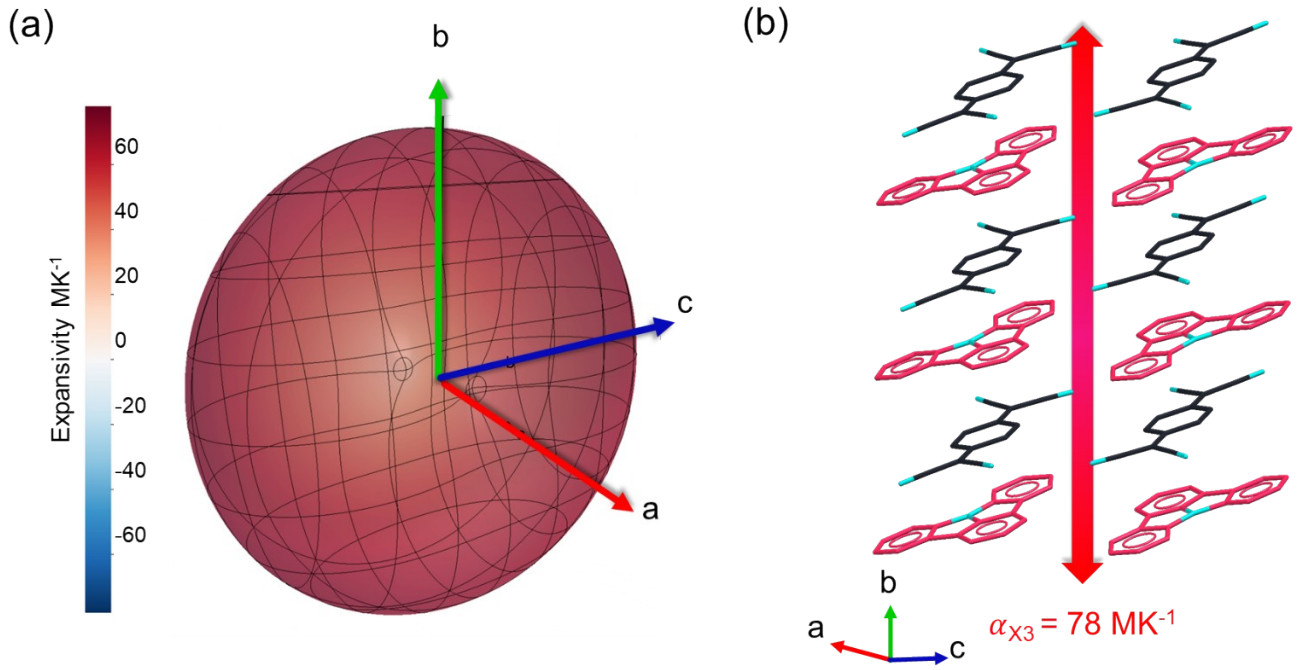

Figure S16. (a) Expansivity indicatrix for **ICZ-TCNQ**. (b) Crystalline packing of **ICZ-TCNQ** seen along the *b*-axis in the direction of the π-stacking between D/A molecules. The TE coefficient is displayed and illustrated with red arrows.

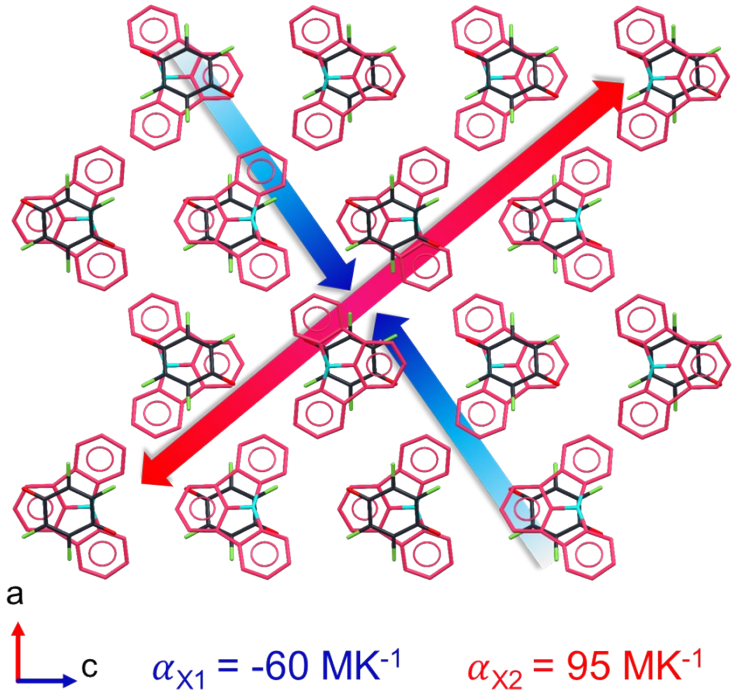

Figure S17. Crystalline packing of **ICZ-TFBQ** seen through the crystallographic *b*-axis (plane *ac*). The TE coefficients are displayed and illustrated with red and blue arrows.

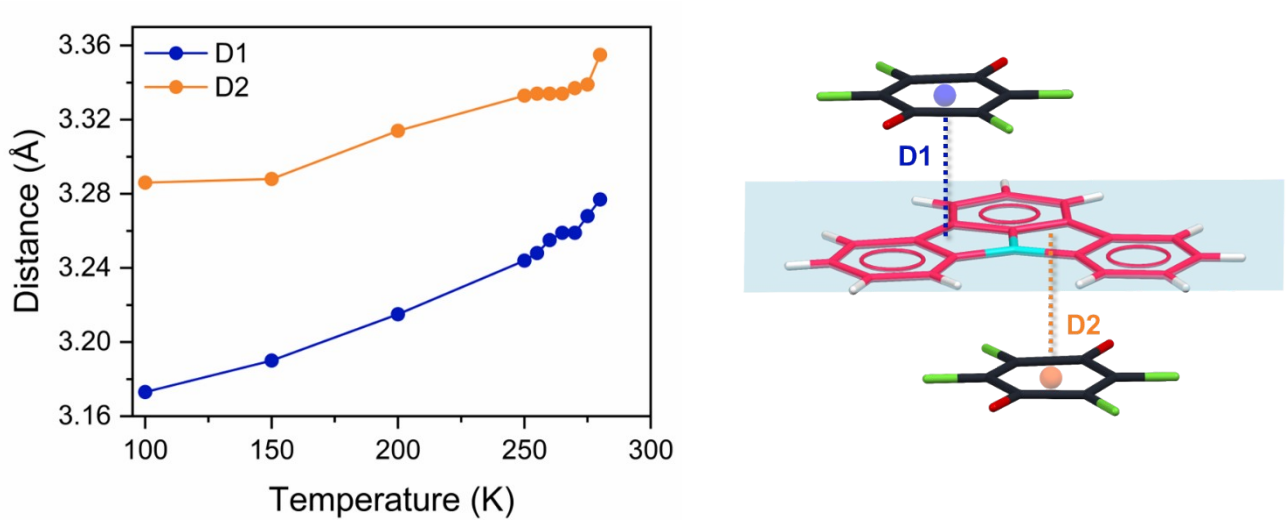

Figure S18. Changes in the π–stacking distances regarding temperature in the cocrystal **ICZ-TFBQ** from 100 K to 280 K.

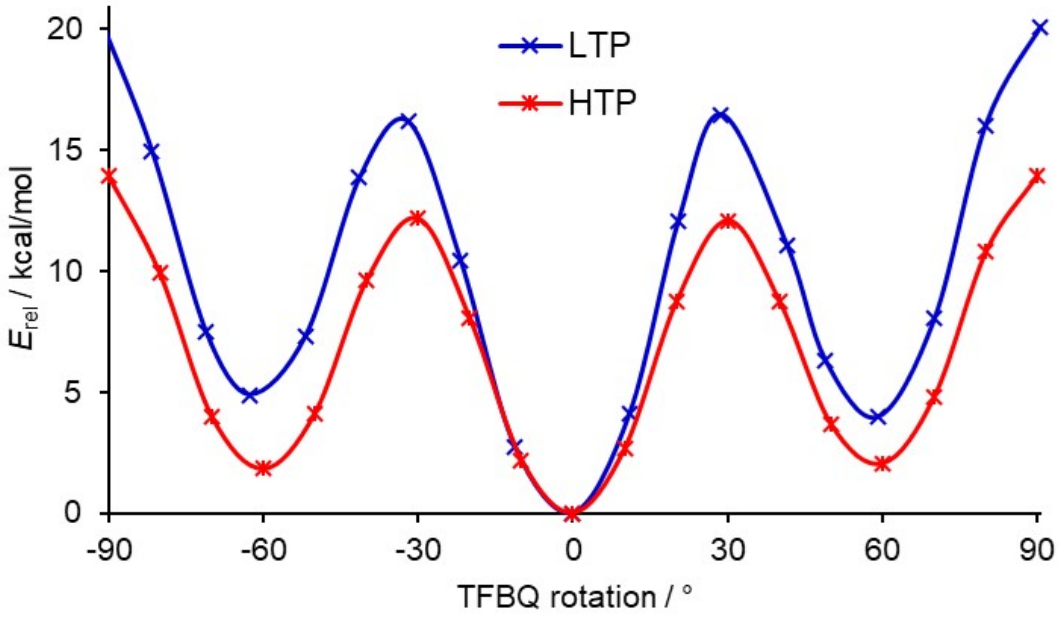

Figure S19. Energetic profile of the 60° rotations of **TFBQ** fragment within the plane in 10° increments.

Table S4. Crystal structure parameters for **ICZ-TCNQ** at 100 K, 200 K and 300 K.

Identification code	**ICZTCNQ-100K**		**ICZTCNQ-200K**		**ICZTCNQ-300K**	
Empirical formula	$C_{18}H_{11}N$, $C_6F_4O_2$		$C_{18}H_{11}N$, $C_6F_4O_2$		$C_{18}H_{11}N$, $C_6F_4O_2$	
Formula weight	445.47		445.47		445.47	
Temperature (K)	100(2)		200(2)		300(2)	
Wavelength (Å)	0.7288		0.7288		0.7288	
Crystal system	Monoclinic		Monoclinic		Monoclinic	
Space group	$P2_1/n$		$P2_1/n$		$P2_1/n$	
Unit cell dimensions	a = 9.1770(9) Å	α= 90°	a = 9.2049(10) Å	α = 90°	a = 9.2145(11) Å	α = 90°
	b = 7.0729(8) Å	β= 96.048(4)°	b = 7.1344(8) Å	β = 96.141(4)°	b = 7.1841(9) Å	β = 96.263(4)°
	c = 32.999(3) Å	γ= 90°	c = 33.241(4) Å	γ = 90°	c= 33.492(4) Å	γ = 90°
Volume (Å^3)	2130.0(4)		2170.4(4)		2203.9(5)	
Z	4		4		4	
Density (mg m^{-3})	1.389		1.363		1.343	
Absorption coefficient (mm^{-1})	0.088		0.087		0.085	
F(000)	920		920		920	
Crystal size (mm^3)	0.500 x 0.030 x 0.010		0.500 x 0.030 x 0.010		0.500 x 0.030 x 0.010	
Theta range for data collection	1.273 to 31.424°		2.302 to 27.929°		2.298 to 26.098°	
Index ranges	-13 ≤ h ≤ 13 -10 ≤ k ≤ 10 -47 ≤ l ≤ 47		-11 ≤ h ≤ 11 -9 ≤ k ≤ 9 -42 ≤ l ≤ 42		-11 ≤ h ≤ 11 -8 ≤ k ≤ 8 -40 ≤ l ≤ 40	
Reflections collected	69025		56733		49261	
Independent reflections	6508 [R(int) = 0.0503]		4780 [R(int) = 0.0662]		4048 [R(int) = 0.0568]	
Completeness to theta = 25.242°	99.8 %		99.8 %		99.7 %	
Absorption correction	Semi-empirical from equivalents		Semi-empirical from equivalents		Semi-empirical from equivalents	
Max. and min. transmission	0.999 and 0.950		0.999 and 0.941		0.999 and 0.938	
Refinement method	Full-matrix least-squares on F^2		Full-matrix least-squares on F^2		Full-matrix least-squares on F^2	
Data / restraints / parameters	6508 / 0 / 316		4780 / 0 / 316		4048 / 0 / 316	
Goodness-of-fit on F^2	1.064		1.049		1.064	
Final R indices [I>2sigma(I)]	R1 = 0.0412 wR2 = 0.1066		R1 = 0.0389 wR2 = 0.0951		R1 = 0.0387 wR2 = 0.0943	
R indices (all data)	R1 = 0.0470 wR2 = 0.1110		R1 = 0.048 wR2 = 0.1021		R1 = 0.0479 wR2 = 0.1006	
Extinction coefficient	n/a		n/a		n/a	
Largest diff. peak and hole (e.Å^{-3})	0.451 and -0.283		0.208 and -0.201		0.148 and -0.175	

Table S5. Crystal structure parameters for **ICZ-TFBQ** at 100 K, 150 K and 200 K.

Identification code	**ICZTFBQ-100K**		**ICZTFBQ-150K**		**ICZTFBQ-200K**	
Empirical formula	$C_{18}H_{11}N$, $C_6F_4O_2$		$C_{18}H_{11}N$, $C_6F_4O_2$		$C_{18}H_{11}N$, $C_6F_4O_2$	
Formula weight	421.34		421.34		421.34	
Temperature (K)	100(2)		150(2)		200(2)	
Wavelength (Å)	0.71073		0.71073		0.71073	
Crystal system	Monoclinic		Monoclinic		Monoclinic	
Space group	$P2_1/c$		$P2_1/c$		$P2_1/c$	
Unit cell dimensions	a = 15.4910(6) Å	α= 90°	a = 15.480(2) Å	α = 90°	a = 15.5166(8) Å	α = 90°
	b = 6.8140(2) Å	β= 91.2360(10)°	b = 6.8416(7) Å	β = 90.887(4)°	b = 6.9014(3) Å	β = 90.931(2)°
	c = 16.6374(6) Å	γ= 90°	c = 16.668(2) Å	γ = 90°	c= 16.7105(10)Å	γ = 90°
Volume (Å^3)	1755.76(11)		1765.1(4)		1789.23(16)	
Z	4		4		4	
Density (mg m^{-3})	1.594		1.586		1.564	
Absorption coefficient (mm^{-1})	0.131		0.130		0.128	
F(000)	856		856		856	
Crystal size (mm^3)	0.359 x 0.356 x 0.338		0.359 x 0.356 x 0.338		0.359 x 0.356 x 0.338	
Theta range for data collection	3.231 to 29.181°		3.219 to 25.246°		3.194 to 29.225°	
Index ranges	-21 ≤ h ≤ 21 0 ≤ k ≤ 9 0 ≤ l ≤ 22		-17 ≤ h ≤ 17 0 ≤ k ≤ 7 0 ≤ l ≤ 19		-21 ≤ h ≤ 21 0 ≤ k ≤ 9 0 ≤ l ≤ 22	
Reflections collected	4797		2503		4838	
Independent reflections	4797 [R(int) = 0.0445]		2503 [R(int) = 0.1635]		4838 [R(int) = 0.0505]	
Completeness to theta = 25.242°	99.4 %		78.3 %		99.4 %	
Absorption correction	Semi-empirical from equivalents		Semi-empirical from equivalents		Semi-empirical from equivalents	
Max. and min. transmission	0.7458 and 0.6912		0.7452 and 0.5986		0.7458 and 0.6842	
Refinement method	Full-matrix least-squares on F^2		Full-matrix least-squares on F^2		Full-matrix least-squares on F^2	
Data / restraints / parameters	4797 / 0 / 281		2503 / 0 / 281		4838 / 0 / 281	
Goodness-of-fit on F^2	1.109		1.214		1.139	
Final R indices [I>2sigma(I)]	R1 = 0.0472 wR2 = 0.1064		R1 = 0.0999 wR2 = 0.2356		R1 = 0.0543 wR2 = 0.1090	
R indices (all data)	R1 = 0.0576 wR2 = 0.1131		R1 = 0.1281 wR2 = 0.2547		R1 = 0.0865 wR2 = 0.1236	
Extinction coefficient	n/a		n/a		n/a	
Largest diff. peak and hole (e.Å^{-3})	0.323 and -0.306		0.401 and -0.375		0.272 and -0.230	

Table S6. Crystal structure parameters for **ICZ-TFBQ** at 250 K, 255 K and 260 K.

Identification code	**ICZTFBQ-250K**		**ICZTFBQ-255K**		**ICZTFBQ-260K**	
Empirical formula	$C_{18}H_{11}N$, $C_6F_4O_2$		$C_{18}H_{11}N$, $C_6F_4O_2$		$C_{18}H_{11}N$, $C_6F_4O_2$	
Formula weight	421.34		421.34		421.34	
Temperature (K)	250(2)		255(2)		260(2)	
Wavelength (Å)	0.71073		0.71073		0.71073	
Crystal system	Monoclinic		Monoclinic		Monoclinic	
Space group	$P2_1/c$		$P2_1/c$		$P2_1/c$	
Unit cell dimensions	a= 15.5003(12)Å	α= 90°	a=15.5007(12) Å	α = 90°	a=15.5010(13) Å	α = 90°
	b= 6.9661(5) Å	β= 91.585(2)°	b=6.9749(5) Å	β = 90.544(2)°	b= 6.9832(5) Å	β = 90.504(2)°
	c= 16.7470(13)Å	γ= 90°	c=16.7557(13) Å	γ = 90°	c=16.7625(14) Å	γ = 90°
Volume (Å^3)	1808.2(2)		1811.5(2)		1814.4(3)	
Z	4		4		4	
Density (mg m^{-3})	1.548		1.545		1.542	
Absorption coefficient (mm^{-1})	0.127		0.127		0.126	
F(000)	856		856		856	
Crystal size (mm^3)	0.394 x 0.346 x 0.342		0.394 x 0.346 x 0.342		0.394 x 0.346 x 0.342	
Theta range for data collection	3.167 to 23.265°		3.164 to 23.281°		3.160 to 23.292°	
Index ranges	-17 ≤ h ≤ 17 -7 ≤ k ≤ 7 -18 ≤ l ≤ 18		-17 ≤ h ≤ 17 -7 ≤ k ≤ 7 -18 ≤ l ≤ 18		-17 ≤ h ≤ 17 -7 ≤ k ≤ 7 -18 ≤ l ≤18	
Reflections collected	11825		11834		11829	
Independent reflections	2454 [R(int) = 0.1299]		2463 [R(int) = 0.1296]		2467 [R(int) = 0.1394]	
Completeness to theta = 25.242°	94.4 %		94.5 %		94.3 %	
Refinement method	Full-matrix least-squares on F^2		Full-matrix least-squares on F^2		Full-matrix least-squares on F^2	
Data / restraints / parameters	2454 / 0 / 280		2463 / 0 / 280		2467 / 0 / 280	
Goodness-of-fit on F^2	1.220		1.247		1.247	
Final R indices [I>2sigma(I)]	R1 = 0.1174 wR2 = 0.2270		R1 = 0.1180 wR2 = 0.2327		R1 = 0.1242 wR2 = 0.2342	
R indices (all data)	R1 = 0.1691 wR2 = 0.2540		R1 = 0.1729 wR2 = 0.2610		R1 = 0.1784 wR2 = 0.2614	
Extinction coefficient	n/a		n/a		n/a	
Largest diff. peak and hole (e.Å^{-3})	0.283 and -0.294		0.262 and -0.384		0.290 and -0.364	

Table S7. Crystal structure parameters for **ICZ-TFBQ** at 265 K, 270 K and 275 K.

Identification code	**ICZTFBQ-265K**		**ICZTFBQ-270K**		**ICZTFBQ-275K**	
Empirical formula	$C_{18}H_{11}N$, $C_6F_4O_2$		$C_{18}H_{11}N$, $C_6F_4O_2$		$C_{18}H_{11}N$, $C_6F_4O_2$	
Formula weight	421.34		421.34		421.34	
Temperature (K)	265(2)		270(2)		275(2)	
Wavelength (Å)	0.71073		0.71073		0.71073	
Crystal system	Monoclinic		Monoclinic		Monoclinic	
Space group	$P2_1/c$		$P2_1/c$		$P2_1/c$	
Unit cell dimensions	a=15.4951(13) Å	α= 90°	a=15.4846(13) Å	α = 90°	a=15.4962(13) Å	α = 90°
	b= 6.9903(5) Å	β= 90.455(2)°	b=6.9953(5) Å	β = 90.398(2)°	b= 7.0097(5) Å	β = 90.350(2)°
	c=16.7629(14) Å	γ= 90°	c=16.7616(14) Å	γ = 90°	c=16.7818(14) Å	γ = 90°
Volume (Å^3)	1815.6(3)		1815.6(3)		1822.9(3)	
Z	4		4		4	
Density (mg m^{-3})	1.541		1.541		1.535	
Absorption coefficient (mm^{-1})	0.126		0.126		0.126	
F(000)	856		856		856	
Crystal size (mm^3)	0.394 x 0.346 x 0.342		0.394 x 0.346 x 0.342		0.394 x 0.346 x 0.342	
Theta range for data collection	3.157 to 23.280°		3.156 to 23.253°		2.427 to 23.276°	
Index ranges	-17 ≤ h ≤ 17 -7 ≤ k ≤ 7 -18 ≤ l ≤ 18		-17 ≤ h ≤ 17 -7 ≤ k ≤ 7 -18 ≤ l ≤ 18		-17 ≤ h ≤ 17 -7 ≤ k ≤ 7 -18 ≤ l ≤18	
Reflections collected	11873		10099		11910	
Independent reflections	2463 [R(int) = 0.1419]		2414 [R(int) = 0.0715]		2472 [R(int) = 0.1363]	
Completeness to theta = 25.242°	94.2 %		92.7 %		94.2 %	
Refinement method	Full-matrix least-squares on F^2		Full-matrix least-squares on F^2		Full-matrix least-squares on F^2	
Data / restraints / parameters	2463 / 0 / 280		2414 / 0 / 280		2472 / 0 / 280	
Goodness-of-fit on F^2	1.243		1.278		1.211	
Final R indices [I>2sigma(I)]	R1 = 0.1329 wR2 = 0.2463		R1 = 0.1220 wR2 = 0.2376		R1 = 0.1279 wR2 = 0.2577	
R indices (all data)	R1 = 0.1914 wR2 = 0.2745		R1 = 0.1685 wR2 = 0.2616		R1 = 0.1911 wR2 = 0.2933	
Extinction coefficient	n/a		n/a		n/a	
Largest diff. peak and hole (e.Å^{-3})	0.276 and -0.295		0.248 and -0.253		0.291 and -0.277	

Table S8. Crystal structure parameters for **ICZ-TFBQ** at 280 K, 285 K and 290 K.

Identification code	**ICZTFBQ-280K**		**ICZTFBQ-285K**		**ICZTFBQ-290K**	
Empirical formula	$C_{18}H_{11}N$, $C_6F_4O_2$		$C_{18}H_{11}N$, $C_6F_4O_2$		$C_{18}H_{11}N$, $C_6F_4O_2$	
Formula weight	421.34		421.34		421.34	
Temperature (K)	280(2)		285(2)		290(2)	
Wavelength (Å)	0.71073		0.71073		0.71073	
Crystal system	Monoclinic		Orthorhombic		Orthorhombic	
Space group	$P2_1/c$		*Pbcn*		*Pbcn*	
Unit cell dimensions	a=15.4906(14) Å	α= 90°	a=7.0361(7) Å	α = 90°	a=7.0399(6) Å	α = 90°
	b= 7.0182(5) Å	β= 90.307(3)°	b=16.8128(18) Å	β = 90°	b= 16.8012(17) Å	β = 90°
	c=16.7875(15) Å	γ= 90°	c=15.5075(17) Å	γ = 90°	c=15.4855(16) Å	γ = 90°
Volume (Å^3)	1825.0(3)		1834.5(3)		1831.6(3)	
Z	4		4		4	
Density (mg m^{-3})	1.533		1.526		1.528	
Absorption coefficient (mm^{-1})	0.126		0.125		0.125	
F(000)	856		856		856	
Crystal size (mm^3)	0.394 x 0.346 x 0.342		0.394 x 0.346 x 0.342		0.394 x 0.346 x 0.342	
Theta range for data collection	2.426 to 23.286°		2.423 to 23.256°		2.424 to 23.256°	
Index ranges	-17 ≤ h ≤ 17 -7 ≤ k ≤ 7 -18 ≤ l ≤ 18		-7 ≤ h ≤ 7 -18 ≤ k ≤ 18 -17 ≤ l ≤ 17		-7 ≤ h ≤ 7 -18 ≤ k ≤ 18 -17 ≤ l ≤ 17	
Reflections collected	10857		8959		9399	
Independent reflections	2465 [R(int) = 0.0819]		1277 [R(int) = 0.1146]		1271 [R(int) = 0.1082]	
Completeness to theta = 25.242°	93.7 %		96.5 %		96.4 %	
Refinement method	Full-matrix least-squares on F^2		Full-matrix least-squares on F^2		Full-matrix least-squares on F^2	
Data / restraints / parameters	2465 / 0 / 281		1277 / 474 / 305		1271 / 456 / 304	
Goodness-of-fit on F^2	1.255		1.916		1.127	
Final R indices [I>2sigma(I)]	R1 = 0.1253 wR2 = 0.2087		R1 = 0.1612 wR2 = 0.4431		R1 = 0.1386 wR2 = 0.2535	
R indices (all data)	R1 = 0.1845 wR2 = 0.2344		R1 = 0.2114 wR2 = 0.4811		R1 = 0.1888 wR2 = 0.2789	
Extinction coefficient	0.021(3)		0.06(3)		n/a	
Largest diff. peak and hole (e.Å^{-3})	0.210 and -0.233		0.334 and -0.367		0.249 and -0.284	

Table S9. Crystal structure parameters for **ICZ-TFBQ** at 295 K and 300 K.

Identification code	**ICZTFBQ-295K**		**ICZTFBQ-300K**	
Empirical formula	$C_{18}H_{11}N$, $C_6F_4O_2$		$C_{18}H_{11}N$, $C_6F_4O_2$	
Formula weight	421.34		421.34	
Temperature (K)	295(2)		298(2)	
Wavelength (Å)	0.71073		0.71073	
Crystal system	Orthorhombic		Orthorhombic	
Space group	*Pbcn*		*Pbcn*	
Unit cell dimensions	a=7.0461(6) Å	α= 90°	a=7.0571(11) Å	α = 90°
	b=16.7994(17) Å	β= 90°	b=16.847(3) Å	β = 90°
	c=15.4702(16) Å	γ= 90°	c=15.534(3) Å	γ = 90°
Volume (Å^3)	1831.2(3)		1846.9(5)	
Z	4		4	
Density (mg m^{-3})	1.528		1.515	
Absorption coefficient (mm^{-1})	0.125		0.124	
F(000)	856		856	
Crystal size (mm^3)	0.394 x 0.346 x 0.342		0.359 x 0.346 x 0.338	
Theta range for data collection	3.135 to 23.270°		3.130 to 28.699°	
Index ranges	$-7 \le h \le 7$ $-18 \le k \le 18$ $-17 \le l \le 17$		$-9 \le h \le 9$ $-22 \le k \le 22$ $-20 \le l \le 20$	
Reflections collected	10264		54036	
Independent reflections	1283 [R(int) = 0.0822]		2373 [R(int) = 0.0451]	
Completeness to theta = 25.242°	97.0 %		98.8 %	
Refinement method	Full-matrix least-squares on F^2		Full-matrix least-squares on F^2	
Data / restraints / parameters	1283 / 366 / 304		2373 / 366 / 305	
Goodness-of-fit on F^2	1.305		1.059	
Final R indices [I>2sigma(I)]	R1 = 0.0987 wR2 = 0.1537		R1 = 0.0487 wR2 = 0.0979	
R indices (all data)	R1 = 0.1552 wR2 = 0.1762		R1 = 0.0953 wR2 = 0.1308	
Extinction coefficient	n/a		0.054(7)	
Largest diff. peak and hole (e.Å^{-3})	0.199 and -0.212		0.140 and -0.138	

References

(S1) Bielecki, A.; Burum, D. P. Temperature Dependence of207Pb MAS Spectra of Solid Lead Nitrate. An Accurate, Sensitive Thermometer for Variable-Temperature MAS. *Journal of Magnetic Resonance, Series A* **1995**, *116* (2), 215–220. https://doi.org/10.1006/jmra.1995.0010.

(S2) Clark, S. J.; Segall, M. D.; Pickard, C. J.; Hasnip, P. J.; Probert, M. I. J.; Refson, K.; Payne, M. C. First Principles Methods Using CASTEP. *Zeitschrift für Kristallographie - Crystalline Materials* **2005**, *220* (5–6), 567–570. https://doi.org/10.1524/zkri.220.5.567.65075.

(S3) Perdew, J. P.; Burke, K.; Ernzerhof, M. Generalized Gradient Approximation Made Simple. *Phys. Rev. Lett.* **1996**, *77* (18), 3865–3868. https://doi.org/10.1103/PhysRevLett.77.3865.

(S4) Vanderbilt, D. Soft Self-Consistent Pseudopotentials in a Generalized Eigenvalue Formalism. *Phys. Rev. B* **1990**, *41* (11), 7892–7895. https://doi.org/10.1103/PhysRevB.41.7892.

(S5) Monkhorst, H. J. Special Points for Brillouin-Zone Integrations. *Phys. Rev. B* **1976**, *13* (12), 5188–5192. https://doi.org/10.1103/PhysRevB.13.5188.

(S6) Tkatchenko, A.; Scheffler, M. Accurate Molecular Van Der Waals Interactions from Ground-State Electron Density and Free-Atom Reference Data. *Phys. Rev. Lett.* **2009**, *102* (7), 073005. https://doi.org/10.1103/PhysRevLett.102.073005.

(S7) Frisch, M. J.; Trucks, G. W.; Schlegel, H. B.; Scuseria, G. E.; Robb, M. A.; Cheeseman, J. R.; Scalmani, G.; Barone, V.; Mennucci, B.; Petersson, G. A.; Nakatsuji, H.; Caricato, M.; Li, X.; Hratchian, H. P.; Izmaylov, A. F.; Bloino, J.; Zheng, G.; Sonnenberg, J. L.; Hada, M.; Ehara, M.; Toyota, K.; Fukuda, R.; Hasegawa, J.; Ishida, M.; Nakajima, T.; Honda, Y.; Kitao, O.; Nakai, H.; Vreven, T.; Montgomery, Jr., J. A.; Peralta, J. E.; Ogliaro, F.; Bearpark, M.; Heyd, J. J.; Brothers, E.; Kudin, K. N.; Staroverov, V. N.; Kobayashi, R.; Normand, J.; Raghavachari, K.; Rendell, A.; Burant, J. C.; Iyengar, S. S.; Tomasi, J.; Cossi, M.; Rega, N.; Millam, J. M.; Klene, M.; Knox, J. E.; Cross, J. B.; Bakken, V.; Adamo, C.; Jaramillo, J.; Gomperts, R.; Stratmann, R. E.; Yazyev, O.; Austin, A. J.; Cammi, R.; Pomelli, C.; Ochterski, J. W.; Martin, R. L.; Morokuma, K.; Zakrzewski, V. G.; Voth, G. A.; Salvador, P.; Dannenberg, J. J.; Dapprich, S.; Daniels, A. D.; Farkas, Ö.; Foresman, J. B.; Ortiz, J. V.; Cioslowski, J.; Fox, D. J. *Gaussian 09 Revision E.01*; Gaussian, Inc.: Wallingford, 2009.

(S8) Becke, A. D. Density-Functional Thermochemistry. III. The Role of Exact Exchange. *Journal of Chemical Physics* **1993**, *98*, 5648–5652. https://doi.org/10.1063/1.464913.

(S9) Lee, C.; Yang, W.; Parr, R. G. Development of the Colle-Salvetti Correlation-Energy Formula into a Functional of the Electron Density. *Phys. Rev. B* **1988**, *37* (2), 785–789. https://doi.org/10.1103/PhysRevB.37.785.

(S10) Sun, L.; Wang, Y.; Yang, F.; Zhang, X.; Hu, W. Cocrystal Engineering: A Collaborative Strategy toward Functional Materials. *Advanced Materials* **2019**, *31* (39), 1902328. https://doi.org/10.1002/adma.201902328.

(S11) Nanova, D.; Beck, S.; Fuchs, A.; Glaser, T.; Lennartz, C.; Kowalsky, W.; Pucci, A.; Kroeger, M. Charge Transfer in Thin Films of Donor–Acceptor Complexes Studied by Infrared Spectroscopy. *Organic Electronics* **2012**, *13* (7), 1237–1244. https://doi.org/10.1016/j.orgel.2012.02.021.

(S12) Ferrari, E.; Mezzadri, F.; Masino, M. Temperature-Induced Neutral-to-Ionic Phase Transition of the Charge-Transfer Crystal Tetrathiafulvalene-Fluoranil. *Phys. Rev. B* **2022**, *105* (5), 054106. https://doi.org/10.1103/PhysRevB.105.054106.

(S13) Navarro-Huerta, A.; Hall, D. A.; Blahut, J.; Gómez-Vidales, V.; Teat, S. J.; Marmolejo-Tejada, J. M.; Dračínský, M.; Mosquera, M. A.; Rodríguez-Molina, B. Influence of Internal Molecular Motions in the Photothermal Conversion Effect of Charge-Transfer Cocrystals. *Chem. Mater.* **2023**, *35* (23), 10009–10017. https://doi.org/10.1021/acs.chemmater.3c01944.